PCCP

ROYAL SOCIETY OF CHEMISTRY

PAPER

View Article Online
View Journal | View Issue

Cite this: *Phys. Chem. Chem. Phys.*, 2022, **24**, 2095

Single-conformation spectroscopy of cold, protonated ^{D}PG-containing peptides: switching β-turn types and formation of a sequential type II/II′ double β-turn†

John T. Lawler, [a] Christopher P. Harrilal,‡[a] Andrew F. DeBlase,§[a] Edwin L. Sibert III,*[b] Scott A. McLuckey*[a] and Timothy S. Zwier*[ac]

Received 23rd October 2021,
Accepted 17th December 2021

DOI: 10.1039/d1cp04852j

rsc.li/pccp

D-Proline (^{D}Pro, ^{D}P) is widely utilized to form β-hairpin loops in engineered peptides that would otherwise be unstructured, most often as part of a ^{D}PG sub-unit that forms a β-turn. To observe whether ^{D}PG facilitated this effect in short protonated peptides, conformation specific IR–UV double resonance photofragment spectra of the cold (~10 K) protonated ^{D}P and ^{L}P diastereomers of the penta-peptide YAPGA was carried out in the hydride stretch (2800–3700 cm^{-1}) and amide I/II (1400–1800 cm^{-1}) regions. A model localized Hamiltonian was developed to better describe the 1600–1800 cm^{-1} region commonly associated with the amide I vibrations. The C=O stretch fundamentals experience extensive mixing with the N–H bending fundamentals of the NH_3^+ group in these protonated peptides. The model Hamiltonian accounts for experiment in quantitative detail. In the ^{D}P diastereomer, all the population is funneled into a single conformer which presented as a type II β-turn with A and ^{D}P in the i + 1 and i + 2 positions, respectively. This structure was not the anticipated type II′ β-turn across ^{D}PG that we had hypothesized based on solution-phase propensities. Analysis of the conformational energy landscape shows that both steric and charge-induced effects play a role in the preferred formation of the type II β-turn. In contrast, the ^{L}P isomer forms three conformations with very different structures, none of which were type II/II′ β-turns, confirming that ^{L}PG is not a β-turn former. Finally, single-conformation spectroscopy was also carried out on the extended peptide [YAA^{D}PGAAA + H]$^+$ to determine whether moving the protonated N-terminus further from ^{D}PG would lead to β-hairpin formation. Despite funneling its entire population into a single peptide backbone structure, the assigned structure is not a β-hairpin, but a concatenated type II/type II′ double β-turn that displaces the peptide backbone laterally by about 7.5 Å, but leaves the backbone oriented in its original direction.

I. Introduction

The structural advantages of utilizing unnatural D-amino acids in biologics-based materials is a well-researched field.[1–3] Their inclusion in molecules reduces susceptibility to enzymatic degradation,[4–6] increases anti-microbial activity,[7–9] and aids in self-assembly of peptide secondary structures.[10,11] Therapeutic peptides are designed with these properties in mind to enhance the efficacy and selectivity of pharmaceuticals.[11,12] Of all the D-amino acids, the effect D-proline has on secondary structure is one of the most significant. Substitution of L-proline with D-proline is known to greatly stabilize β-turn formation in peptides.[13–18] This finding has been heavily exploited by synthetic organic chemists to produce scaffolds for drug delivery through the inclusion of a ^{D}PX moiety (X = Ala or Gly) in peptides.[15,16,19]

The terminology surrounding the classification of different types of "turns" in peptide biochemistry is quite complex.[20,21] Turns are first categorized by the separation between residues i and i + n that form a hydrogen bond. For example, an α-turn involves an $i \rightarrow i + 4$ hydrogen bond.[22] In simple terms, this means there is a separation between the first and last amino acids forming the turn of four peptide bonds. Similarly, a γ-turn utilizes an $i \rightarrow i + 2$ hydrogen bond, with two peptide bonds between interacting residues,[23,24] while β-turns have

[a] *Department of Chemistry, Purdue University, West Lafayette, Indiana 47907-2084, USA. E-mail: tszwier@sandia.gov, mcluckey@purdue.edu*
[b] *Department of Chemistry, University of Wisconsin-Madison, Madison, WI 53706, USA. E-mail: elsibert@wisc.edu*
[c] *Gas Phase Chemical Physics, Sandia National Laboratories, Livermore, CA 94550, USA*

† Electronic supplementary information (ESI) available. See DOI: 10.1039/d1cp04852j

‡ Present address: Pacific Northwest National Laboratories, Richland, WA, USA.
§ Present address: Spectral Energies, LLC, Dayton, OH, USA.

Table 1 Turn type and Ramachandran angles for the most observed β-turn motifs

Turn type	Ramachandran angles (degrees) (ϕ_{i+1}, ψ_{i+1}; ϕ_{i+2}, ψ_{i+2})
Type I	(−60, −30), (−90, 0)
Type I′	(+60, +30); (+90, 0)
Type II	(−60, +120); (+80, 0)
Type II′	(+60, −120); (−80, 0)

$i \rightarrow i+3$ H-bonds. Turns are then further classified by the (ϕ,ψ) Ramachandran dihedral angles present in the turning region.[20,22]

β-turns are the most common of all the turns present in native proteins.[20,25] Ramachandran angles (ϕ,ψ) can be used to group β-turns into different types, of which types I, II, I′, and II′ are the most prominent.[26] Table 1 compares the Ramachandran angles of the prominent turn types of interest here. Types I/I′ and II/II′ are mirror images of one another, with the unprimed versions more common. However, type I′ and II′ β-turns are of particular interest, since they become the preferred turns in β-hairpins, protein structural elements that cause a reversal in the direction of the protein backbone to form antiparallel β-strands. Studying the origin and intramolecular contributions to the stability of these turns is therefore important to understanding and utilizing larger, antiparallel beta strands.[20,25–27]

A powerful method to study the inherent conformational preferences of these scaffolds is to analyze them in the gas phase where the lack of solvent interactions lays bare the intramolecular hydrogen bonds that stabilize these structures.[28–31] In the past, our group has leveraged the power of IR–UV double resonance techniques to probe the ^{D}P and ^{L}P diastereomers of $[YAPAA + H]^+$ and the $[YG^{L}PAA + H]^+$ peptide ions in the gas phase.[32,33] A central question we sought to address is whether the presence of a charge would promote or inhibit secondary structure formation in short peptides such as this. We also sought to understand how stereochemical changes affected these preferences.

The observed conformations were surprisingly sensitive both to the proline stereochemistry and the A ↔ G exchange. Based on the spectroscopy, we assigned structures to two conformers of $[YA^{D}PAA + H]^+$, one a charge-stabilized type II′ β-turn and the other a double γ-turn. $[YA^{L}PAA + H]^+$ did not form the mirror image type II β-turn, as one might have imagined, but an unstructured turn anchored by a *cis*-Pro. When the methyl side chain of Ala(2) was replaced by Gly, the preference for *trans*-amide at Pro returned, as did the formation of a type II′ β-turn, but the position of the turn shifted to $G^{L}P$ in $YG^{L}PAA$ from ^{D}PA in $YA^{D}PAA$.[32,33]

Two major questions remained after the previous studies. First, is the ^{D}PG sequence an even stronger β-turn forming sequence, like it is in solution? None of the previous peptides had directly incorporated this turn-forming sequence, so here we study $[YA^{D}PGA + H]^+$, which does. We chose to keep the peptide length the same as in previous studies so as to enable a direct comparison with that work. As before, the structure-forming propensities of the peptide backbone must be accommodated in the presence of the NH_3^+ group present at the N-terminus, without the screening effects of H_2O as solvent. We compare the results on $YA^{D}PGA$ to those on its diastereomer $YA^{L}PGA$.

Second, in longer peptides, does the ^{D}PG moiety produce a β-hairpin anchored by the ^{D}PG β-turn? Additional hydrogen bonding, brought about through the extension of the peptide backbone, may support the formation of the β-hairpin through the formation of a β-sheet like structure that is more energetically favorable than its unstructured competitors. Extending the peptide also could move the charge site further away from the turn which may help to elucidate the role charge plays in influencing its formation. To answer these questions, we studied the model peptide $[YAA^{D}PGAAA + H]^+$ as a gas phase ion *via* cold ion spectroscopy.

Cold ion spectroscopy is well-suited to 3D structural determination of ions in the gas phase, as the frequencies of the vibrations report directly on their hydrogen-bonding architectures.[30,34,35] It has been utilized to examine the structure of compounds of varied types, from sugars to peptides, providing incisive tests of theory and new structural insights.[30] Cooling ions down to 10 K removes internal energy from the ion, stabilizing each conformation in its vibrational zero-point level and sharpening the vibrational transitions. In the hydride stretch region (2800–3700 cm^{-1}), the vibrational frequencies shift in response both to their local hydrogen-bond donor environment and their coupled motion with other vibrations, reporting on the specific H-bonding architecture of the ion. The amide I/II regions provide a complementary picture of these hydrogen bonds from the point of view of the H-bond acceptors (amide I, C═O group) or the stiffening of the NH bends (amide II).

In this work, we compare the experimental single-conformation IR spectra with the predictions of calculations to obtain structural assignments. While this comparison could be carried out using scaled harmonic vibrational frequencies and IR intensities, here we develop and incorporate a local mode description of the NH_3^+ bends that come into the 1600–1800 cm^{-1} region and mix with the amide I vibrations. This largely unrecognized contribution to the spectrum made scaled harmonic calculations inappropriate. As we will see, the local mode approach leads to much better fits to the experimental spectra, strengthening the conformational assignments.

II. Methods

A. Experimental

All spectroscopic data were taken on a custom-built instrument for cold ion spectroscopy, previously described.[29,36] Concisely, the design is that of a triple quadrupole mass spectrometer in which an orthogonal spectroscopy axis was added between the second ($q2$) and third ($q3$) quadrupoles, all of which are held at room temperature with helium as collisional gas for trapping. Ions are generated *via* nano-ESI, stored in an initial quadrupole ion trap (QIT, $q0$) for about 30 ms before being turned onto the

triple quad axis, where they are stored in the second QIT ($q2$) where the ions of interest are isolated *via* RF/DC isolation. This apex isolation could also serve to thermally anneal the gas phase ions. The ion packet is then steered through a turning quadrupole and down the spectroscopy axis where it is trapped in an octupole trap that is cooled to 5 K *via* a closed-cycle helium cryostat (Sumitomo Heavy Industries, Tokyo, Japan). After cooling to $\sim$10 K *via* collisions with the He buffer gas, the ions are spectroscopically interrogated *via* a tunable UV laser (ScanMatePro dye laser frequency doubled by an Inrad Autotracker III). The created photofragments are then extracted back down the spectroscopy axis and turned into a quadrupole for analysis in either ''spectroscopy mode'' or ''mass spectrometry mode''. In mass spectrometry mode, a mass spectrum of the photofragments is generated *via* mass-selective axial ejection.[37] The ''spectroscopy mode'' entails ejection of remaining precursor ions with SX wave software followed by dumping of all remaining photofragments onto a channeltron detector (4773G, Photonis USA).

UV action spectra are recorded by monitoring the total photofragment signal as a function of laser wavenumber. Upon obtaining a UV spectrum and identifying transitions that may be due to different ion conformations, conformation-specific IR spectra are taken by employing IR–UV double resonance techniques.[32]

In IR–UV depletion spectroscopy, the UV laser wavelength is fixed on a transition of interest in the UV spectrum creating a steady signal of photofragment ions due to the monitored conformation. A Nd:YAG-pumped IR parametric converter (LaserVision) is spatially overlapped but temporally precedes the UV laser by 200 ns is scanned in wavelength. Upon absorption of an IR photon by the conformer of interest, a fraction of the population is removed from the ground state, thereby broadening and shifting its UV absorption. This results in a depletion in the total photofragment signal from the single conformation being monitored in the UV. Tuning the IR laser while monitoring this depletion gives a single-conformer IR spectrum.

IR–UV hole-burning spectroscopy employs the same experimental arrangement but fixes the IR laser wavelength on a unique IR absorption of the conformer of interest, while wavelength of the UV laser source is tuned. The difference spectrum with and without the IR present provides a conformer-specific UV spectrum.

B. Solution preparation

Solutions of $YA^{D}PGA$, $YA^{L}PGA$, and $YAA^{D}PGAAA$ (Genscript) were prepared in 50 : 50 methanol : water solvent at a concentration of 200 μM and electrosprayed to create the corresponding protonated ion.

C. Computational

Conformational searches were performed for gas-phase $[YA^{D}PGA + H]^+$, $[YA^{L}PGA + H]^+$ and $[YAA^{D}PGAAA\ H]^+$ structures using the Monte Carlo multiple minimum method with the AMBER* and OPLS3 force fields inside the MACROMODEL software package.[38] Approximately 1000 unique structures for the isolated ion were found between the two force fields for each of the molecules. To narrow down the potential structures further, the 1000 structure pool was clustered into sub-groups with closely similar peptide backbone RMSD. The centroid of each of the sub-groups was then optimized at the B3LYP/6-31+G(d)-GD3BJ level of theory[39–42] using Gaussian16 and harmonic vibrational frequencies/intensities were calculated to obtain predicted infrared spectra to compare with experiment.[43] In early tests of the workflow, we ran DFT calculations on every member of each sub-group and deduced that there weren't measurable differences in the IR spectra in the hydride stretch and amide I/II regions between members of the same sub-group. As a result, we focus attention in what follows on the unique peptide backbone architectures in making assignments, ignoring simple sidechain rotamer conformations.

To correct for anharmonicity the calculated spectra were scaled by 0.958 for the NH, CH, and OH stretching regions, 0.973 for the free OH transitions, and 0.970 for Amide II. Adjusting the calculated transitions by these scale factors puts them into agreement with previously calculated and fitted spectra.[29,32,33]

The region of the infrared typically associated with the amide I vibrations (C═O stretch fundamentals of the amide group, 1600–1800 cm^{-1}) was handled separately, since in peptides protonated at the N-terminus, the NH_3^+ bends occur in the same region. These transitions also carry oscillator strength comparable with the amide I vibrations and are mixed with them. As a result, simply applying separate scale factors to the NH_3^+ bends and C═O stretches is not correct since the coupling between them is significant.

In order to apply separate scalings, we transform to a localized representation obtained as an orthogonal transformation of those normal modes in the above frequency window. The resulting localized modes are readily classified as either NH_3^+ bends (not including the umbrella mode), phenyl C–C stretches or C═O stretches, thus allowing for a separate scaling of the frequencies associated with those modes. The C–C stretch normal modes are localized on the benzene ring and carry little oscillator strength, so we do not discuss them further. The scalings are based on fitting to conformer A of $[YA^{L}PGA + H]^+$ and are found to be 0.976 for the amide I vibrations and 0.942 for the NH_3^+ bends. The former scaling was determined by fitting to the highest frequency mode in this region which corresponds to the C═O stretch of the carboxylic acid.[44]

''Stick'' spectra were generated for the centroid of each cluster. These calculated spectra were then matched to the experimental spectrum and the best fit centroids were found. All conformational minima within each cluster with best fit centroids that lie within 10 kJ mol^{-1} of the global minimum in internal energy were then optimized using DFT at the same level of theory used for the centroids. Unique structural identifiers in the single conformer infrared spectra (*e.g.*, tyrosine OH, carboxylic acid OH) were used to assign the structure that best fit both the NH stretch and amide I/II regions. Spectral matching

in conjunction with energy sorting led to assignments of the observed conformation associated with each spectrum, as described in Section III. Free energy calculations were carried out on all structures lying within +20 kJ mol^{-1} of the global minimum in internal energy. This provided predictions for the equilibrium populations in the room temperature quadrupole ion traps in which initial thermal equilibrium of the gas phase ions is likely achieved.

III. Results and analysis

A. UV spectra of $[YA^{D}PGA + H]^{+}$ and $[YA^{L}PGA + H]^{+}$

Cold UV action spectra of $[YA^{D}PGA + H]^{+}$ and $[YA^{L}PGA + H]^{+}$ were recorded by monitoring their complete photofragmentation signal as a function of laser wavelength (Fig. 1). A striking difference in the complexity of the two UV spectra is immediately evident. $[YA^{D}PGA + H]^{+}$ produces a simple UV spectrum with two intense bands (35 611 and 35 632 cm^{-1}) that each support short Franck–Condon progressions in modes of frequency 13 and 24 cm^{-1}. We postulate that the two intense bands are electronic origins from two conformers that have identical peptide backbone architectures but differ in the orientation of the OH group on the Tyr, as observed in other similar protonated peptides.[33] The UV spectrum of $[YA^{L}PGA+ H]^{+}$ is far more complex, containing multiple unique transitions that point to the presence of multiple conformations.

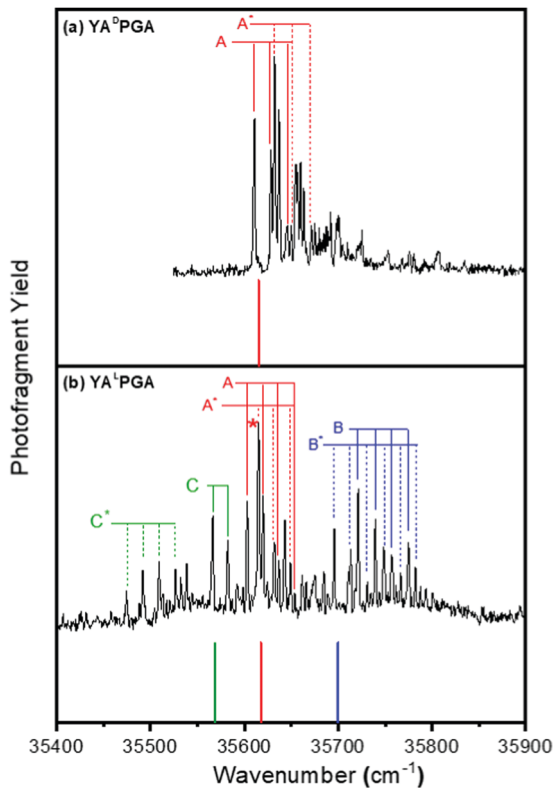

Fig. 1 UV spectra of $YA^{D}PGA$ and $YA^{L}PGA$. UV action spectra of (a) $[YA^{D}PGA + H]^{+}$ and (b) $[YA^{L}PGA + H]^{+}$. The origins and Franck–Condon progressions of the different conformers are labelled A, B, and C with the asterisk denoting transitions due to tyrosine rotamers of the conformer. Below each UV spectrum is a colored stick denoting the TD-DFT calculated (M052X/6-31+g(d)) electronic origin of the assigned conformation, after scaling by 0.8443. See text for further discussion.

To ascertain the identity of the conformations present in these spectra, IR–UV double resonance techniques were employed. Identification of transitions in the UV spectra due to unique conformers was carried out by first obtaining conformation specific infrared spectra of several of the most intense peaks in the spectra, including transitions labelled A and A′ in Fig. 1(a) and A, A′, B, B′, C, and C′ in Fig. 1(b). Conformation specific UV spectra were then obtained using IR–UV holeburning spectroscopy (Section II.A). In the case of $[YA^{D}PGA + H]^{+}$, the hole-burning spectrum with IR hole-burn laser at 3394 cm^{-1} contained all significant transitions in the UV action spectrum (Fig. S1, ESI†). The corresponding spectra of $[YA^{L}PGA + H]^{+}$ (Fig. S2, ESI†) prove the presence of three conformers labeled in Fig. 1(b). The primed and unprimed labels shown in Fig. 1 denote transitions due to the two OH rotamers of the Tyr UV chromophore.

Note that the electronic origin and vibronic structure of conformer A of $[YA^{L}PGA + H]^{+}$ is at a UV wavelength nearly identical to that of the single conformer of $[YA^{D}PGA + H]^{+}$. Furthermore, the vibronic structure is also very similar. This provides evidence that the UV chromophore is in a similar environment in these two diastereomeric conformers.

Fig. 1 also contains predictions of the relative S_0–S_1 origins based on vertical TD-DFT calculations at the M052X/6-31+g(d) level of theory. The conformations used for these calculations are those assigned based on the infrared spectra which is to follow. The results of these calculations are all scaled by 0.8443, a scale factor chosen so as to bring the S_0–S_1 origin of the single conformer of $[YA^{D}PGA + H]^{+}$ into alignment with experiment. The excellent correspondence between experiment and these predictions adds confirming evidence to the conformational assignments. Similar calculations were used with success in previous studies as a check on the assignments.[32]

B. Conformation-specific infrared spectrum of $[YA^{D}PGA + H]^{+}$

Fig. 2(b) presents the conformation-specific infrared spectrum of the single observed conformer of $[YA^{D}PGA + H]^{+}$ in the hydride stretch region. Below the experimental spectrum is the calculated spectrum for the global minimum conformer, which closely matches the experimental spectrum. The spectrum of $[YA^{D}PGA + H]^{+}$ should have XH stretch transitions due to the Tyr and carboxylic acid OH groups, three amide NH groups, and three transitions due to the NH stretches of the NH_3^{+}. The free OH stretch region (3550–3700 cm^{-1}) shows a characteristic Tyr free OH stretch near 3648 cm^{-1} but lacks the free OH stretch of the carboxylic acid group, which is known to occur at 3571 cm^{-1}.[45] The presence of the free Tyr OH is in keeping with the difficulty in engaging the OH group in the *para* position on the aromatic ring directly with the rest of the ion in a peptide of this size. The absence of the free OH stretch at 3571 cm^{-1} points to the carboxylic acid OH group serving as donor in a hydrogen bond that shifts the OH stretch fundamental to lower frequency. Since other bands are accounted for,

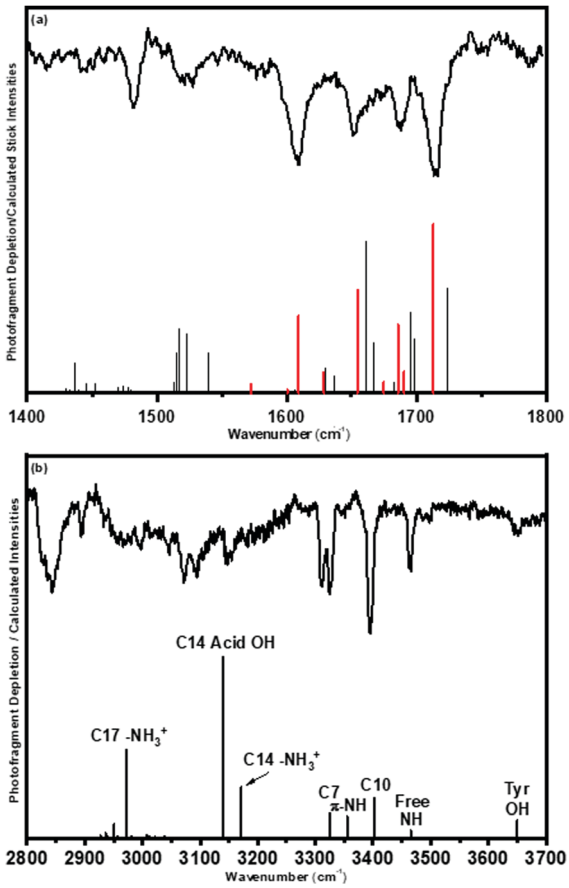

Fig. 2 IR spectrum of YA^{D}PGA with calculated sticks. (a) Corresponding experimental and calculated spectra in the 1400–1800 cm^{-1} region. The black stick spectra are the results of a harmonic treatment using a single scale factor for all vibrations in the 1600–1800 cm^{-1} region, while the red stick spectra are those resulting from the local mode Hamiltonian model. See text for further discussion. (b) Conformation specific infrared spectrum of the single conformer of [YA^{D}PGA + H]$^{+}$ (black) in the hydride stretch region, compared to the calculated vibrational frequencies and infrared intensities of the best-fit conformation, which is also the global minimum.

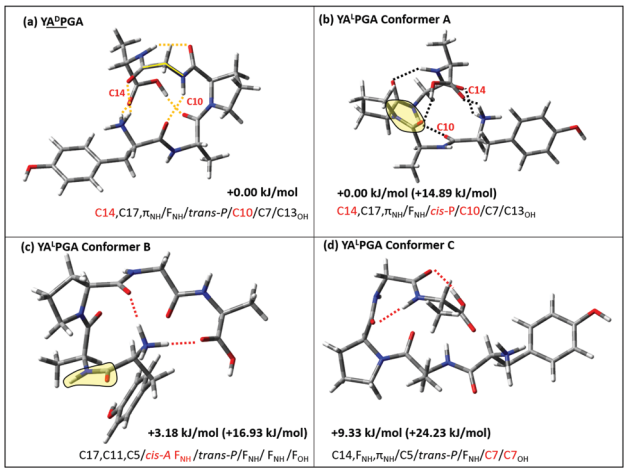

Fig. 3 Assigned conformations of (a) [YA^{D}PGA + H]$^{+}$, and (b–d) the three assigned conformers of [YA^{L}PGA + H]$^{+}$. A summary of the H-bonding architecture in terms of the size H-bonded rings formed, starting from the N-terminus NH_3^+. Relative energies are given comparing within a given diastereomer, with the comparison across diastereomers given in parentheses.

this carboxylic acid OH stretch must be in a strong H-bond that shifts its frequency below 3200 cm^{-1}. The NH stretch region (3200–3500 cm^{-1}) directly probes the peptide backbone hydrogen bonding network, with its three amide NH groups. The free NH stretch region (3450–3500 cm^{-1}) contains a single peak at 3465 cm^{-1}, while the bound NH stretch region has three resolved transitions, with the most intense at 3394 cm^{-1} followed by two closely spaced peaks at 3324 and 3310 cm^{-1}.

This conformer must therefore contain one free NH group and three other NH groups in moderately strong H-bonds. The assigned structure shown in Fig. 3(a) possesses the best-fit stick spectrum shown below the experimental spectrum. In the calculated structure, the free NH is associated with Ala(2). This amide group's C=O (the Tyr C=O) is engaged in a C10 hydrogen bond with the glycine NH opposite it, appearing at 3394 cm^{-1}. This constitutes a type II β-turn involving the A^{D}P rather than the ^{D}PG segment of the peptide. The remaining hydrogen bound NH stretch transitions involve an NH_3^+-π interaction at 3324 cm^{-1} and a C7 hydrogen bond at 3310 cm^{-1} that is formed between the Pro C=O and the amide NH of Ala(5).

The spectrum of [YA^{D}PGA + H]$^{+}$ in Fig. 2(b) possesses very broad transitions in the 2800–3100 cm^{-1} region, implying the existence of strong hydrogen bonds to either the acid OH, charged amine, or both, mirroring the broad absorptions found in previous studies.[32] The scaled harmonic calculations in this region tend to underestimate the shift to lower frequency, but the patterns tend to hold. Based on the calculations, the C17 NH_3^+ stretch is likely responsible for the intense band at 2843 cm^{-1} in the experimental spectrum, while the OH stretch of the COOH group (which forms a C13 H-bond with the Ala(2) C=O) and C14 NH_3^+ transitions produce the broad absorptions that stretch from 2950–3200 cm^{-1}.

The corresponding IR spectrum in the amide I/II region is shown in Fig. 2(a). The spectrum lacks any transitions above 1720 cm^{-1}, indicating that the COOH carbonyl group is in a strong H-bond, since it is typically found above 1750 cm^{-1} in the absence of a H-bond. Furthermore, there is a strong transition at 1661 cm^{-1}, an unusually low frequency for even a strongly H-bonded amide I vibration. The calculated spectra using a single scale factor typical of the amide I region (0.980) leads to the prediction in black, which is a poor match particularly of the 1661 cm^{-1} transition. However, implementation of the local mode Hamiltonian involving the three NH_3^+ bending modes and five amide I fundamentals leads to a predicted spectrum shown in red that is in significantly better agreement with experiment. This adds confidence that the assigned structure is the one observed experimentally.

C. Conformation-specific infrared spectra of [YA^{L}PGA + H]$^{+}$

1. Conformer A. The IR–UV double resonance spectrum of conformer A of [YA^{L}PGA + H]$^{+}$ was recorded with the UV laser fixed on the transition marked with a red asterisk in Fig. 1(b).

IR spectra were also recorded with UV fixed on corresponding transitions marked as due to A′, and were identical to those due to A. The conformer-specific IR spectrum that results (Fig. 4) bears an over-all resemblance to that of the sole observed conformer of $[YA^{D}PGA + H]^{+}$ (Fig. 2). Comparison of the experimental spectrum to the calculated spectrum of the global minimum structure for $[YA^{L}PGA+ H]^{+}$ shows a reasonable fit in the 3200–3500 cm^{-1} region, and we argue below for this global minimum structure as that responsible for the spectrum. Of the eight conformations with energies within 10 kJ mol^{-1} of the global minimum, half present with a free acid OH group that is absent in the spectrum of conformer A. Of the bound acid conformations only the assigned global minimum structure accurately matches the two largest transitions in the experimental spectrum. A more detailed analysis of the uniqueness of the experimental fit follows.

As in the ^{D}P analog, the spectrum in Fig. 4(d) displays a free Tyr OH at 3650 cm^{-1}, while missing the free carboxylic acid OH stretch, indicating that the latter group is involved in a H-bond. Fig. 3(b) shows the assigned structure responsible for the calculated spectrum shown in Fig. 4(d). The calculated spectrum possesses a set of three transitions in the 3300–3400 cm^{-1} region. The experimental spectrum shows just two resolved transitions in this region at 3308 and 3385 cm^{-1} which are both unusually broadened. We postulate that the broadened, asymmetric shape of the band at 3308 cm^{-1} is due to the presence of two unresolved transitions. The calculated transition at 3307 cm^{-1} is due to a C7 H-bonded NH stretch between the proline carbonyl and the NH of the C-terminal alanine group, while the transition calculated at 3320 cm^{-1} is associated with an NH_3^{+}-π NH stretch. The transition at 3385 cm^{-1} is assigned to a C10 hydrogen bond between the glycine NH and the tyrosine carbonyl oxygen. Just to the higher frequency side of this transition in the experimental spectrum are a set of three closely spaced transitions, where the calculations show just a single free NH stretch (3445 cm^{-1}). The two additional bands could arise from overlap in the UV with vibronic bands due to the other conformers that contribute to the UV photofragment signal at the UV wavelength used to probe conformer A. However, the frequencies of the transitions (3423, 3447, and 3464 cm^{-1}) do not line up with those due to the other conformers. Instead, we postulate that the extra pair of transitions are

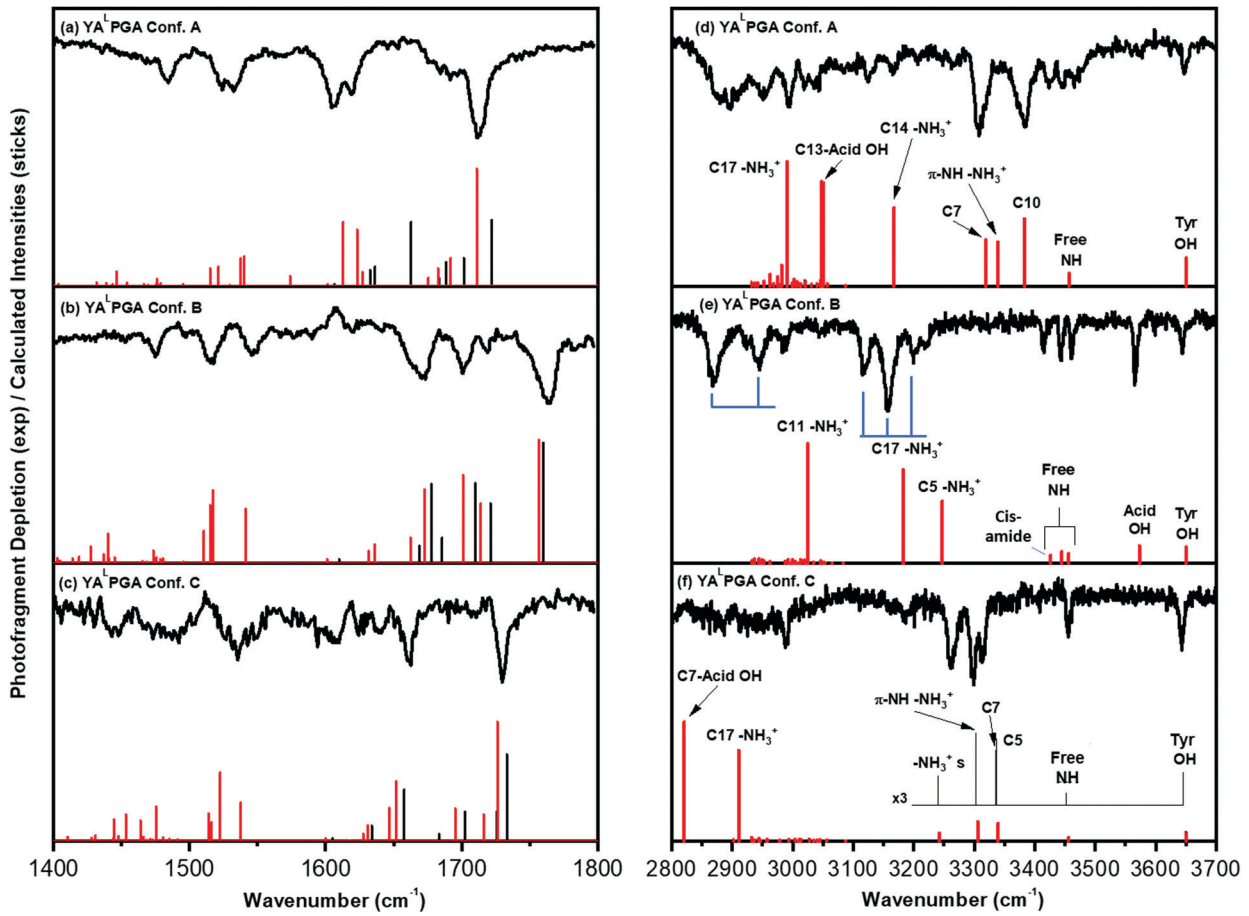

Fig. 4 Conformation Specific Infrared Spectra of $[YA^{L}PGA + H]^{+}$. (a–c) Corresponding experimental and calculated spectra in the 1400–1800 cm^{-1} region. The black stick spectra are the results of a harmonic treatment using a single scale factor for all vibrations in the 1600–1800 cm^{-1} region, while the red stick spectra are those resulting from the local mode Hamiltonian model. See text for further discussion. (d–f) Conformation specific infrared spectrum of the three observed conformers of $[YA^{L}PGA + H]^{+}$ (black) in the hydride stretch region, compared to the calculated vibrational frequencies and infrared intensities of the best-fit conformations.

combination bands involving the C7 and C10 NH stretches with a low-frequency vibration that couples to it.

The region from 2800–3200 cm^{-1} has broad absorption characteristic of strong H-bonds involving the H-bonded COOH and NH_3^+ groups. Due to their breadth and the sub-structure that appears on top of them (*e.g.*, due to the CH stretch fundamentals), we are not able to make firm assignments of these transitions, but simply note that broadened versions of the assigned stick spectra match the over-all shape of the broad absorption. The acid OH stretch is shifted down to around 3000 cm^{-1} due to its involvement in a C13 H-bond with the carbonyl oxygen of the Ala(2) residue. The broad, structured absorption in the experimental spectrum is accounted for by this C13 OH stretch and two strong H-bonds involving the NH_3^+ group.

Since the fit for YA^LPGA conformer A in the NH stretch region is not fully secure, we sought additional confirmation based on the IR spectrum in the amide I/II regions (1400–1800 cm^{-1}), which is shown in Fig. 4(a). Using the local mode Hamiltonian for the combined C=O stretch/NH_3^+ bends, the match between experiment and calculation is excellent. Inclusion of the bends is especially important here because the NH_3^+ scissors is especially intense in this conformer, for reasons we do not fully understand.

The assigned structure for conformer A of YA^LPGA, shown in Fig. 3(a), is a close analog of the sole conformer of YA^DPGA, incorporating a β-turn that is further stabilized by the H-bond of the COOH OH group to the central amide C=O of the β-turn. The NH_3^+ group is also in a similar binding pocket to that in YA^DPGA, engaging in two strong H-bonds with the Gly(3) and carboxylic acid C=O groups. However, a notable difference with the β-turn in YA^DPGA is that conformer A of YA^LPGA incorporates a *cis* Pro that enables a similar H-bonding architecture despite the change in chirality of the Pro C(α). This leads to differences in the strengths of the H-bonds involving NH_3^+. Further comment on this structure will be taken up in the discussion.

2. Conformer B. In stark contrast to the complex H-bonded network of conformer A, the spectrum of conformer B is consistent with a structure that largely lacks amide NH stretch H-bonds. In particular, there is a trio of free amide NH stretches (3460, 3443, and 3416 cm^{-1}), signaling that none of the backbone amide NH groups in the molecule is involved in hydrogen bonding. Furthermore, both the Tyr OH stretch (3648 cm^{-1}) and carboxylic acid OH stretch (3566 cm^{-1}) are free. While such a structure would seem energetically unfavorable, the lowest energy structure that matches these criteria, shown in Fig. 3(b), is only 3.2 kJ mol^{-1} above the global minimum. Its only H-bonds are due to the NH_3^+ group burying itself in a pocket created by the C-terminal half of the molecule.

Since the carboxylic acid OH group is free, it doesn't produce a broad absorption in the 2800–3200 cm^{-1} region, and therefore reveals the absorptions due to the NH_3^+ group particularly clearly. A weak C5 hydrogen bond between the charged amine and the adjacent carbonyl group on the tyrosine residue is calculated to be the highest frequency of the three $NH_3^+\cdots O{=}C$ H-bonds. The other two NH_3^+ hydrogen bonds are similar to those in conformer A and YA^DPGA, involving a C17 NH_3^+ hydrogen bond to the C-terminal carbonyl and a C11 hydrogen bond to the proline carbonyl. All three of these fundamentals show Franck–Condon like combination bands built off them, as indicated by tie lines in Fig. 4(e). Their presence indicates a strong coupling of these NH_3^+ NH stretch modes to low frequency motions of the binding pocket. They are displayed clearly in the present spectrum, but are also likely to be present in the broad, structured absorptions of conformer A.

The charge-stabilizing pocket for the NH_3^+ group in $[YA^LPGA + H]^+$ conformer B is made possible because the first amide group from the N-terminus is a *cis*-amide rather than *trans*, marked in yellow in Fig. 3(c). Its free amide NH stretch is at 3416 cm^{-1}, lower in frequency than is typical for a *trans* amide (3450–3490 cm^{-1}). This frequency shift constitutes a signature of the presence of a *cis*-amide group. The *cis*-amide motif has previously been observed in solution phase structures of small peptides and occurs most often in amide bonds adjacent to proline residues, as it is here.[46,47] To our knowledge this is the first non-proline *cis*-amide conformation discovered by cold ion spectroscopy.

The single-conformer IR spectrum in the 1400–1800 cm^{-1} region is shown in Fig. 4b. Once again, the local mode Hamiltonian that correctly handles the mixing of the NH_3^+ bends and C=O stretch fundamentals produces an excellent fit to experiment, further securing the assignment. The free COOH transition is at 1774 cm^{-1}, well above that of the other transitions.

3. Conformer C. Fig. 4(c) displays the IR–UV double resonance spectrum of conformer C of $[YA^LPGA + H]^+$ in the hydride stretch region. The spectrum displays a free Tyr OH (3650 cm^{-1}) and lacks a free carboxylic acid OH, as was the case in conformer A. A single free NH stretch transition appears at 3454 cm^{-1}, while three resolved, H-bonded NH stretch transitions are observed in the 3250–3350 cm^{-1} region. Since the free OH stretch is missing, the COOH must be in a H-bond, which could involve a *trans* COOH conformation, as is the case in several other protonated peptides[32,33] In conformer C, there is a broad absorption over the 2800–3100 cm^{-1} region, which is less intense and shows less structure than in conformer A. The sharp band at 2988 cm^{-1} is present in all three conformers and is likely an alkyl CH stretch transition shared by all three.

The tentatively assigned spectrum for conformer C is shown as a stick spectrum in Fig. 4(f), due to the structure shown in Fig. 3(d). The fit is reasonably good, but the structure is calculated to be 9.33 kJ mol^{-1} above the global minimum in free energy, a result that is hard to reconciliate with its presence, a result we will address briefly in the discussion.

Nevertheless, the calculated spectrum nicely reproduces the triad of bound NH stretch fundamentals, has a single free amide NH stretch, and a bound carboxylic OH stretch. That this latter transition is predicted to be at 2820 cm^{-1} may mean that its absorption is shifted below 2800 cm^{-1}, and also that it will be very broad. The single free NH stretch belongs to the glycine NH. The NH stretch region contains the often-observed NH-π

interaction of the NH_3^+ (3320 cm^{-1}), but also incorporates three transitions not observed in the previous conformers. A set of closely spaced transitions belonging to C7 and C5 hydrogen bonds are recognized adjacent to the NH-π transition. The C7 cycle is formed between the C-terminal Ala NH and the ^{L}Pro carbonyl, whereas the C5 H-bond is formed between the N-terminal Ala NH interacting with its carbonyl oxygen. A pseudo-C5 hydrogen bond is also formed by the charged amine and the adjacent carbonyl on the Tyr residue. The only macrocycle H-bond involving the NH_3^+ group is a C17 H-bond to the carbonyl on the C-terminus. This same C17 H-bond is present in all three conformers of YA^{L}PGA, but with varying strengths. In $[YA^LPGA + H]^+$ conformer C, the H-bond distance is only 1.60 Å.

The spectrum of conformer C in the amide I/II region is shown in Fig. 4(c). The local mode Hamiltonian fit is quite good over-all. An interesting feature of this conformer is that the NH_3^+ vibrations in this frequency region carry very little oscillator strength and do not mix with the amide I vibrations. The strong transition at 1726 cm^{-1} is principally due to the C=O of the carboxylic acid, while the band at 1650 cm^{-1} is, according to the calculation, an unresolved doublet that consists of two amide I bands, the brighter of the two forming a hydrogen bond with the OH group on the carboxylic acid.

D. Peptide length and β-turn formation: $[YAA^DPGAAA + H]^+$

By extending the peptide chain on either side of the D-proline residue we hope to elucidate the effect of charge and chain length on the stabilization of the turn. To this end the protonated peptide $[YAA^DPGAAA + H]^+$ was subjected to single-conformation spectroscopy.

The UV photofragmentation spectrum of $[YAA^DPGAAA + H]^+$ in the S_0–S_1 origin region is shown in Fig. 5. The spectrum is remarkably simple, with a single dominant electronic origin transition at 35 818 cm^{-1} followed by several weak vibronic bands built off it. That such a large peptide would fold into a single structure already suggests strongly that the ^{D}PG turn-forming region provides strong structure-directing influence on this peptide sequence. Notably, the electronic origin of $[YAA^DPGAAA + H]^+$ is shifted ~200 cm^{-1} to the blue of its smaller chain counterpart $[YA^DPGA + H]^+$, reflecting greater interaction between the phenol ring of tyrosine with its protonated peptide surroundings. As with the shorter peptides, we carried out TD-DFT calculations on the assigned structure, with the prediction included in Fig. 5 after scaling with the same scale factor used in Fig. 1. The close correspondence provides confirming evidence for the assigned structure. The phenol rotamer of this structure is predicted to be about 60 cm^{-1} blue-shifted from the first. While there are transitions in this region, they are much weaker than the main origin. This would imply some cooling of the phenol rotamer population in the cold trap.

Fig. 6 shows the single conformer IR spectrum in the hydride stretch (Fig. 6b) and mid-IR regions (Fig. 6a) while monitoring the UV photofragment signal at the S_0–S_1 origin.

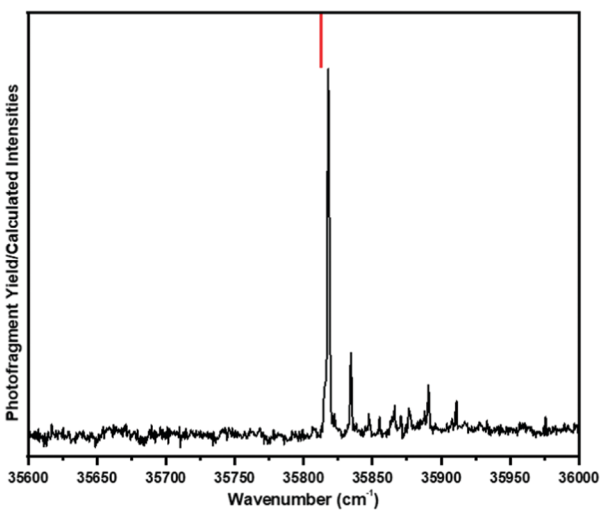

Fig. 5 UV photofragment spectrum of cryo-cooled $[YAA^DPGAAA + H]^+$ in the S_0–S_1 origin region with corresponding TD-DFT calculated electronic origin of assigned conformation in red.

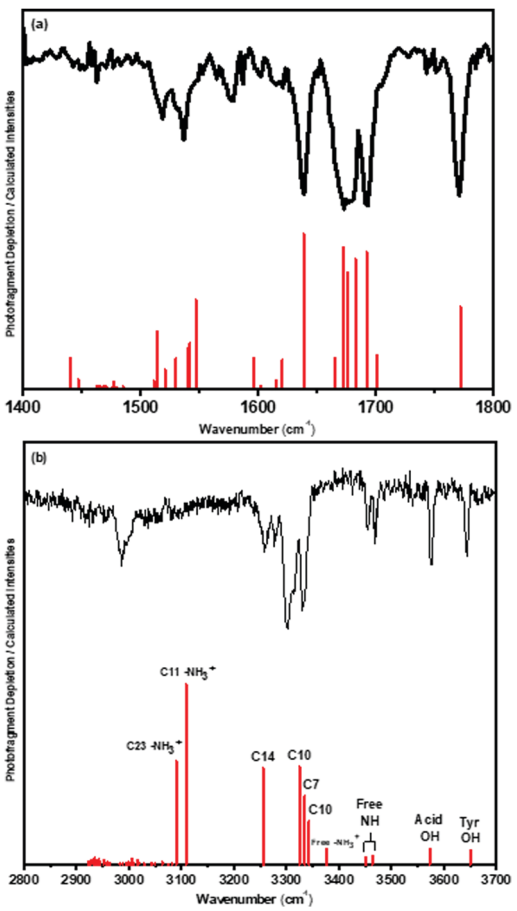

Fig. 6 Infrared spectrum of $[YAA^DPGAAA + H]^+$. (a) Corresponding experimental and calculated spectra in the 1400–1800 cm^{-1} region using the local mode Hamiltonian model. (b) Conformation specific infrared spectrum of the single observed conformer of $[YAA^DPGAAA + H]^+$ (black) in the hydride stretch region, compared to the calculated vibrational frequencies and infrared intensities of the best-fit conformation, which is also the global minimum.

The experimental spectrum is extremely simple, given the size of the protonated peptide, and is dominated by a collection of transitions in the 3240–3350 cm^{-1} region. Unlike its shorter ^{D}PG analog, [YAA^{D}PGAAA + H]$^{+}$ has both a free Tyr OH (3650 cm^{-1}) and a free carboxylic acid OH (3576 cm^{-1}). Notably, the spectrum contains two well-resolved free amide NH stretch transitions at 3451 and 3463 cm^{-1}, indicating that two of the amide groups are also not involved in H-bonds.

After an extensive search (Section II.X), the single conformation shown in Fig. 7 was identified as meeting the structural criteria and was also calculated to have the lowest free energy at 298 K. This choice of temperature matches the temperature of the quadrupole ion trap used for mass selection of the parent ion in our experiment.

The calculated spectrum for this conformer matches experiment satisfactorily well in the 3200–3700 cm^{-1} region, possessing the free Tyr OH, free acid OH, and two free amide NH stretch transitions. The triad of transitions between 3300–3350 cm^{-1} is replicated by one C7 and two C10 amide NH stretch fundamentals. The single calculated absorption at 3255 cm^{-1} ascribed to a C14 NH stretch is tentatively assigned to one of the pair of transitions at 3258 and 3277 cm^{-1} in the experimental spectrum, likely appearing in Fermi resonance with the overtone of the 1640 cm^{-1} transition present in the amide I/NH_3^+ bend region (Fig. 6b). Given the size and complexity of this longer peptide, it is especially important to have verification of the structural assignment based on spectra recorded in more than one frequency region. To that end, we recorded the single-conformer spectrum in the 1400–1800 cm^{-1} region shown in Fig. 6a. As anticipated based on the NH stretch region, there is a strong transition due to the free COOH carbonyl at 1772 cm^{-1}. Beyond this, the spectrum has a dense set of transitions in the 1650–1700 cm^{-1}, and a single strong transition at 1639 cm^{-1}. As with the shorter peptides, we implemented a local mode Hamiltonian model that included the mixing between NH^{3+} bends and C=O stretch fundamentals. In this case, the NH^{3+} bends are somewhat lower in frequency and the mixings smaller, so that the results of the local mode model are qualitatively similar to those from a scaled harmonic calculations. Nevertheless, the calculated spectrum closely matches experiment, strengthening the case for assignment of the carrier of the spectra to the conformer of [YAA^{D}PGAAA + H]$^{+}$ shown in Fig. 7.

IV. Discussion

We have presented single-conformation IR spectra of [YAPGA + H]$^{+}$ containing both d-Pro and l-Pro, and of the longer analog [YAA^{D}PGAAA + H]$^{+}$. In this section we focus on the assigned conformations and what they tell us about the conformational preferences and the structure-defining properties of the ^{D}PG sequence and the site of charge, the N-terminal NH_3^+. Since a major point of comparison is with previous studies of YAPAA and YGPAA, we present in Table 2 a summary of the backbone structures, turn stabilization, and charge pockets involved in the series.

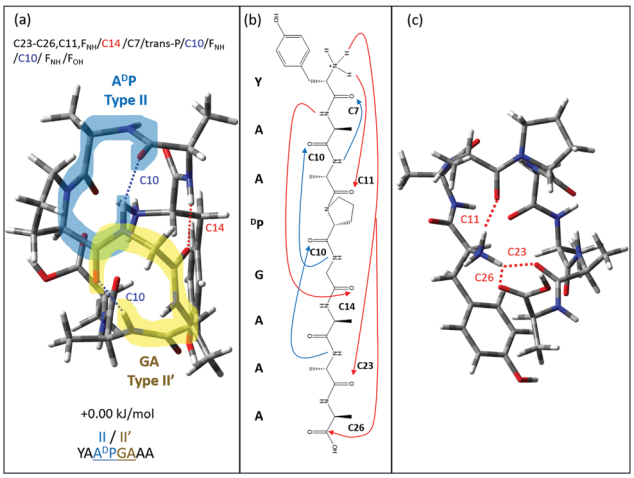

Fig. 7 (a) Calculated lowest energy structure of [YAA^{D}PGAAA + H]$^{+}$ showing the sequential β-turns from a side view. The individual turns are highlighted in blue and yellow. (b) Stick structure with highlighted hydrogen bonding pattern. A red arrow indicates an N-to-C terminal NH···O=C hydrogen bond while a blue arrow is indicative of the opposite. (c) Top-down view of the structure highlighting the binding pocket surrounding the NH_3^+.

A. Formation of a gas phase type II β-Turn in [YA^{D}PGA + H]$^{+}$

In a recent study of the conformational preferences of [YAPAA + H]$^{+}$ by DeBlase *et al.* some of us showed that the ^{D}P diastereomer produced a type II′ β-turn, while the ^{L}P diastereomer did not.[32] In that case, steric overlap between the Ala(2) methyl group and the ^{L}P ring destabilized type II′ β-turn formation in YA^{L}PAA and led to formation of a *cis*-amide group at ^{L}P. The importance of steric effects was confirmed by removing the methyl group to form YG^{L}PAA and showing that this change recovered type II′ β-turn formation. At the same time, even YA^{D}PAA had a second conformer with similar population that was not a type II′ β-turn.

In the present work, we hypothesized that combining ^{D}P with Gly(4), would produce the type II′ β-turn exclusively, as this ^{D}PG sequence is the one used by peptide chemists seeking to build type II′ β-turn formation into peptide sequences.[14,15,17] The type of turn can best be determined through examination of the Ramachandran angles forming the turn. Inspection of these angles in the assigned structure indicates that [YA^{D}PGA + H]$^{+}$ forms a type II β-turn and not the expected type II′ turn (Table 1). Furthermore, the position of the turn is around A^{D}P and not ^{D}PG. This result is inconsistent with the notion that the ^{D}PG moiety locks in a type II′ β-turn and therefore induces β-hairpin formation.

To better elucidate a possible explanation for type II β-turn formation, it is helpful to compare the structure and spectrum of [YA^{D}PGA + H]$^{+}$ to previously reported spectra of [YA^{D}PAA + H]$^{+}$ which forms a type II′ β-turn.[32] As the type II and II′ β-turns have the opposite sense (*i.e.*, dihedrals of opposite sign, Table 1) but are otherwise identical, the spectroscopic signatures of the two types of turns should be similar. This is evident when comparing the IR spectra of the observed conformer of [YA^{D}PGA + H]$^{+}$ to that of conformer B of [YA^{D}PAA + H]$^{+}$

Table 2 Compilation of secondary structure motifs, turn stabilizations, and charge pockets for the studied set of ions containing β-turns

Ion	Backbone structure	Turn stabilization	Charge pocket
^{D}PG	Type II′ β-hairpins in solution	NA	NA
YGGFL[29]	Type II′ β-turn/β-hairpin	C10, C14	C11, C17, π_{NH}
YA^{D}PAA[32]	Conf. B = type II′ β-turn Conf. A = γ–γ	Conf. B = C10, C14 Conf. A = C7, C7	Conf. B = C11, C17, π_{NH}; Conf. A = C14, C17, π_{NH}
YA^{L}PAA[32]	Charge-stabilizing loop, *cis*-Pro amide bond	C14, C17	C14, C17, π_{NH}
YG^{L}PAA[32]	Type II′ β-turn	C10, C14	C14, C17, π_{NH}
YA^{D}PGA	Type II β-turn/β-hairpin	C10, C14	C14, C17, π_{NH}
YA^{L}PGA	A = *cis*-Pro β-turn B = *cis*-amide charge-stabilizing loop C = γ-C7	A = C10, C14 B = C11, C17 C = C7, C7	A = C14, C17, π_{NH} B = C17, C11, C5 C = C14, F_{NH}, π_{NH}

(Fig. S3, ESI†). Both contain the nominal structural framework of a β-turn, with its C10 hydrogen bond, and a C14 H-bond that represents the first rung of the β hairpin.

However, not only is the type turn opposite to that expected, but the placement of the proline residue in the turn that forms this hydrogen bond is across A^{D}P rather than ^{D}PG. In [YA^{D}PAA + H]$^{+}$ the proline residue lies in the classic $i + 1$ position, putting it at the front of the turn where it anchors the formation of the turn. By contrast, in [YA^{D}PGA + H]$^{+}$, the proline takes up the $i + 2$ position at the end of the turn. In re-positioning the β-turn in [YA^{D}PGA + H]$^{+}$, the C14 H-bond that constitutes the first rung of the β hairpin involves a H-bond from the NH_3^+ rather than NH$\cdots$O=C, as it is in protonated YA^{D}PAA.

To understand these differences, we compared the free energies of YA^{D}PGA and YA^{D}PAA conformations for the two types of turn structures (II and II′) positioned either as ^{D}PX or A^{D}P. In YA^{D}PGA, the type II A^{D}P β-turn is lower in energy by some 14.3 kJ mol^{-1} than the type II′ ^{D}PG turn we anticipated forming. By contrast, in YA^{D}PAA the observed type II′ ^{D}PA turn is nearly isoenergetic with the alternative type II A^{D}P structure (ΔE = 0.54 kJ mol^{-1}). This close energetic proximity raises the question of why both turn types weren't observed in protonated YA^{D}PAA. Indeed, in YAPAA there was a minor conformer (labeled conformer D) that was identified by an IR–UV gain spectrum but whose spectrum we couldn't disentangle.[32] With the YA^{D}PGA type II spectrum in hand, we now see that this type II β-turn was a likely assignment for this minor conformer of YA^{D}PAA.

As the only difference between the two molecules is the presence/absence of the A4 methyl group, the reason for the energetic difference between the structures may lie in the interactions that predominate in its absence. With the A4 methyl group removed in YA^{D}PGA the A5 NH and the carbonyl from the proline residue form a C7 hydrogen bond that was prevented in YA^{D}PAA by the steric hinderance that would be created by the nearby methyl group. This C7 hydrogen bond in YA^{D}PGA turns the end of the molecule on itself, positioning the acid OH group so that it can form a hydrogen bond with the A2 carbonyl. This stabilization mechanism near the C-terminal end of YA^{D}PGA is then the likely reason that an A^{D}P type II β-turn is preferred over its ^{D}PG type II′ counterpart.

B. Lengthening the peptide to [YAA^{D}PGAAA + H]$^{+}$

Our initial goal in studying the octapeptide [YAA^{D}PGAAA + H]$^{+}$ was to place the β-turn forming ^{D}PG sequence at the center of a longer peptide to catalyze type II′ β-turn formation. We argued that, by distancing the turn from the protonated amine in the sequence, its role as a β-turn former would be unveiled, and perhaps lead to formation of a longer β hairpin even in the presence of the protonated amine. Experimentally, we observed a single conformer with a beautifully sparse UV spectrum and infrared spectra that were also remarkably uncongested, suggesting formation of a very stable structure. After a detailed search of conformational space, the global minimum structure was indeed very stable, with four amide–amide H-bonds that also accommodated incorporation of the NH_3^+ moiety in a stable binding pocket.

However, instead of a single β-turn at the ^{D}PG sequence, the global minimum structure incorporated two back-to-back β-turns: a type II turn subtending the A^{D}P unit concatenated to a type II′ turn involving GA. An analysis of the conformational families observed provides a window into the exceptional stability of this molecule. Of the 700+ structures ascertained by the conformational search; sixty conformational families resulted. Energetic sorting *via* DFT calculations placed the assigned structure as the global minimum with six other structures remaining in the lowest 10 kJ mol^{-1}. The sequential turn motif dominated in all six of these structures which speaks to its stability. Half of the six structures, constituting the higher energy conformations, contained no bound acid OH moiety, a structural component that is easily identifiable in the experimental spectrum. The lack of this transition in the calculated spectrum meant that these structures could not be candidates. The three remaining structures had closely similar calculated spectra in the XH stretch and amide I/II regions, implying a high degree of structural similarity. Nevertheless, the pattern of transitions in the experimental spectra is best matched by the global minimum structure both in ΔE and ΔG (298 K).

Having observed this sequential turn motif, we wondered if it was present more generally in peptides. A recent study by Dunbrack *et al.* of over 1000 ultra-high resolution PDB structures constituting over 13 000 β-turns sheds light on the prevalence of not only the β-turn but on the sequential turn motif.[48] Analysis of the loop regions of these proteins revealed that β-turns make up 63% of these regions and of the β-turns present, type II/II′ turns constitute ~20% of the population. These numbers are consistent with the importance of the β-turn as a structural motif for turning the protein backbone. Notably, 64% of β-turns overlap with another

β-turn. However, the sequential type II/II′ turns observed in $[YAA^{D}PGAAA + H]^{+}$ is quite rare, as a small number of double turns (~6%) begin with either a type II or II′ turn with an even smaller number (<1%) being concatenated turns of the type we observe.

Fig. 7a shows a side-on view of the assigned structure of $[YAA^{D}PGAAA + H]^{+}$, highlighting the concatenation of the two β-turns, which span five amide groups, with the amide group 3 that spans ^{D}PG shared between the two, with its NH group serving as H-bond donor in the type II β-turn and its C═O as acceptor in the type II′ β-turn. The sequential turn motif begins with a type II $A^{D}P$ β-turn anchored by a C10 hydrogen bond between the G5 amine and A1 carbonyl. Critical to the structure is the orientation of the G5 amide as its bond to the A1 carbonyl positions the P4 carbonyl perfectly for the formation of the C10 of the type II′ turn that follows. The essential nature of the initial type II turn is enhanced in that it also supports the first rung of a β-hairpin, a C14 H-bond between A2 amine and G5 carbonyl. This G5 carbonyl is also the middle amide group in the type II′ β-turn, and therefore stabilizes the II/II′ sequential β-turn structure as a whole.

This sequential β-turn motif has clear spectral signatures. There is a 'belt' of three amide groups 1, 3, and 5 involved in the β-turn H-bonds, whose NH bonds (two of which are C10 and one C7) point in the same direction and produce coupled NH stretch modes of very similar frequency. These modes are responsible for the intense, congested set of transitions between 3300–3350 cm^{-1} (Fig. 6b). The effect of a single β-turn is to turn the peptide backbone back on itself so that, after the turn, it travels in the opposite direction. Interestingly, the inclusion of a sequential turn shifts the direction of the protein back to the original direction with a displacement in the lateral direction by about 7.5 Å.

Vital to the structure of any gas phase ion is the effect of the charge site, in this case the protonated N-terminus. With three possible hydrogen bond donors, the NH_3^+ charge site can be a significant perturbation to the secondary structure of a peptide or add to its stabilization. In $[YAA^{D}PGAAA + H]^{+}$, the charge works positively with the secondary structure to secure the sequential β-turn motif. Fig. 7(c) shows a close-up view of the binding pocket formed around the NH_3^+ group and the three hydrogen bonds in which it is engaged in. The first pair of hydrogen bonds involves a single NH being shared between the A7 carbonyl and the acid carbonyl. This effectively ties the two ends of the peptide together keeping the remaining portions of the backbone in proximity and facilitating bonding. The remaining NH group forms a C11 H-bond to the A3 carbonyl, which is the central amide in the type II β-turn, adding to the stability of this turn. Combining the sequential turn and tight bonding of the charge site is undoubtedly important to maintaining the overall structure of the molecule in the gas phase. The final result is a compact structure whose two β-turns of opposite sense would typically have central amide groups that are not involved in peptide H-bonds. Here, we see that they are stabilized by H-bonds involving the first rung of the β-hairpin and the charged N-terminus.

C. Conformational complexity of $[YA^{L}PGA + H]^{+}$

Our study of $YA^{L}PGA$ was motivated in part by the test it could provide of the ^{D}PG sequence as a β-turn former. By changing the chirality of Pro in the sequence, we can see how the conformational preferences respond. We hypothesized that, even in the gas phase protonated ion, $YA^{L}PGA$ would be less directed towards the type II/II′ β-turn than its d-Pro diastereomer. This was borne out by the single-conformer UV and IR spectra of $[YA^{L}PGA + H]^{+}$ that reveal the presence of three conformers with significant population, none of which form type II/II′ β-turns. It is also important to note that the global minimum in energy/free energy in $[YA^{L}PGA + H]^{+}$ is 14.9 kJ mol^{-1} less stable than the $[YA^{D}PGA + H]^{+}$. While both these results are a significant verification of our hypothesis, we seek to understand these differences by looking in more detail at the YALPGA structures that are formed.

1. Conformer A: A *cis*-proline β-turn. Conformer A is the structure of $[YA^{L}PGA + H]^{+}$ closest to the type II/II′ β-turn, which can be classified nominally as a β-turn, with a C10 H-bond spanning the $A^{L}P$ sequence (Fig. 4b), exactly as it is positioned in $YA^{D}PGA$ (Fig. 4d). Indeed, the infrared spectra of $YA^{L}PGA$ (A) and $YA^{D}PGA$ are reasonably similar, consistent with the two conformers possessing the same H-bonding architecture, labeled as C14, C17, π_{NH}/F_{NH}/Pro/C10/C7/$C13_{OH}$ in Fig. 4. Conformer A retains the Pro in the $i + 2$ position of the turn as a means of reducing steric strain from the A2 methyl group. The charge site is also similar, anchoring the C-terminal end of the molecule in two ways. First, it forms a C14 hydrogen bond with the G4 carbonyl which composes the second rung of what would be a β-hairpin. The charged amine also forms a strong C17 hydrogen bond with the A5 carboxylic acid carbonyl. This hydrogen bonding pattern ties the N-terminal and C-terminal ends of the peptide together while leaving the portion of the peptide involved in the β-turn free from its direct influence.

However, the $YA^{L}PGA$ structure is not a type II/II′ β-turn, for the simple reason that the Pro itself is a *cis*-proline. In trying to understand how the same hydrogen bonding pattern could lead to a different structure it is important to consider the effect of the stereochemistry change of the proline. The difference in these structures lies in the distortion of the backbone that occurs around ^{L}P in conformer A, which twists in such a way as to destroy the bond angles necessary to classify the turn as a type II β-turn. The bond angles instead are nominally consistent with a type IV β-turn, a catch-all classification that includes all turns that have the hydrogen bonding pattern of a β-turn but lack the specific angles of the other numbered turns. However, formation of the β-turn is only made possible in the l-Pro diastereomer by the presence of the *cis*-Pro in the turn. Since proline has no NH group to involve in H-bonding directly, the presence of the *cis*-Pro is seen most clearly in the shift to lower frequency by 16 cm^{-1} in the C═O stretch of Gly, producing a doublet where there is a single transition in $[YA^{D}PGA + H]^{+}$ type II β-turn.

While the energetic preference of all the amino acids favors *trans*-amides over *cis*, proline is known to have the smallest energy difference, and therefore to appear commonly in proteins (~5%).

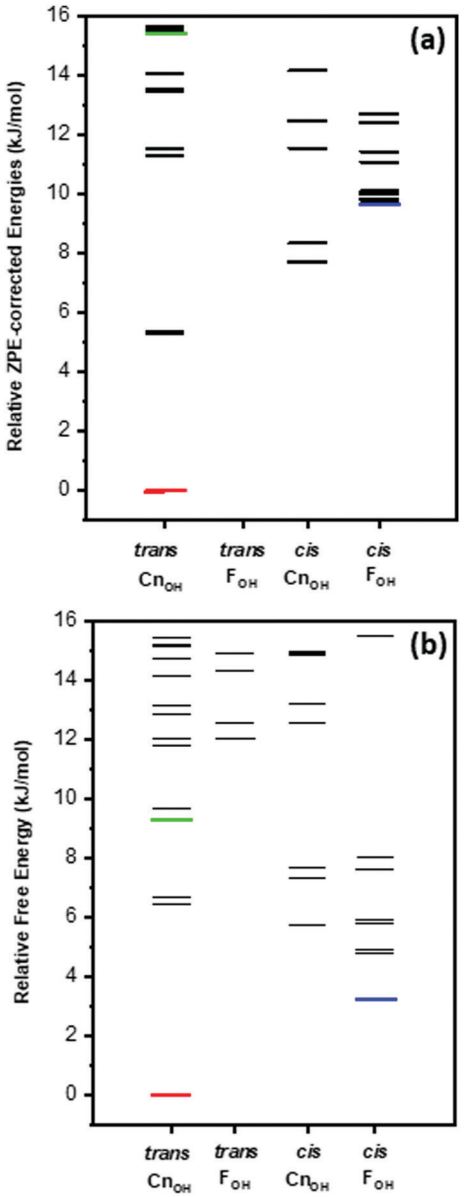

Fig. 8 (a) Relative energies at 0 K, including vibrational zero-point energy corrections, for the conformers of $[YA^{L}PGA + H]^{+}$. The horizontal axis divides the structures into groups based upon the presence or absence of a *cis* amide bond in the non-Pro amino acids (*cis*/*trans*) and whether the acid OH is in a hydrogen bond (Cn_{OH}) or not (F_{OH}). Each line in the figure represents the energy of a calculated structure while the energies of the three conformers that have best fits to the observed conformers are shown in red (conformers A), blue (conformer B), and green (conformer C). (b) Gibbs Free Energy (ΔG 298 K) level diagram for $[YA^{L}PGA + H]^{+}$ with relative energy on the *y*-axis. The lines labeled in red (conformer A), blue (conformer B), and green (conformer C) mark the energies of the best fit structures to each infrared spectrum.

It is therefore not surprising that the *cis*-Pro motif is observed in the gas phase. Previous studies of the analogous peptides $[YA^{D}PAA + H]^{+}$ and $[YG^{L}PAA + H]^{+}$ observed similar *cis*-Pro structures.[32] Fig. 8(a) plots the relative energies of the low-lying conformers of $[YA^{L}PGA + H]^{+}$, while Fig. 8(b) displays the relative free energies at 298 K. Interestingly, this unusual β-turn involving *cis*-Pro is the global minimum in both plots. This happens despite the energetic penalty of *cis*-Pro, which seems to push against the claim that ^{D}PG forms β-turns preferentially relative to ^{L}PG.

2. Conformer B: incorporation of a *cis*-amide bond not involving proline. The conformer specific infrared spectrum of conformer B of $[YA^{L}PGA + H]^{+}$ was quite unusual in having three free amide NH stretch transitions, and a free carboxylic acid OH stretch. This indicated very little peptide backbone hydrogen bonding in the structure. The conformation assigned to conformer B is one in which H-bonds to the NH_3^{+} dominate in forming a tight binding pocket around an otherwise loosely held loop. The effect of the charge is so dominant as to overcome any influence the proline may have on locking in a β-turn. The structure of conformer B, shown in Fig. 3(c), is presented in an orientation that highlights the dominant role played by the NH_3^{+} group, with three C=O groups on the C-terminal end of the peptide pointing towards the NH_3^{+} group.

This structure is made possible by the presence of a *cis*-amide bond between the Y1 and A2 residues, a counter-intuitive result given that *cis*-amides are formed at an energetic penalty of about 8.8 kJ mol^{-1}.[49] To test this conclusion the exact same structure was built in Gaussian, but replacing the *cis*-amide with a *trans*-amide bond. After optimization, the *trans* amide structure was found to be 34.7 kJ mol^{-1} higher in energy than its *cis* counterpart.

The question that then remains is why the *cis* amide structure of Fig. 3(b) is so low in energy, just +3.2 kJ mol^{-1} above the global minimum. First, conformer A also has a *cis*-amide, but in that case involving Pro. As a result, the energy difference based on this alone would be the energy difference between these two *cis*-amide groups. Second, while the NH_3^{+} binding pocket in conformer B is similar to that in A (with C11 and C17 H-bonds to it), H-bond distances are smaller in the Y1–A2 *cis* amide isomer, implying stronger hydrogen bonds and a more stable NH_3^{+} binding pocket in conformer B than A.

Finally, it is worth noting that *cis*-amide containing structures dominate the low energy portion of the conformational landscape of $[YA^{L}PGA + H]^{+}$. Indeed, after the all *trans*-amide global minimum structure of conformer A, the next six most stable structures in free energy all contain a *cis* amide bond between Y1–A2. The observation of non-proline containing *cis* amide bonds in the conformational landscape of this peptide is one of the significant results from this work.

3. Conformer C. A tentative conformational assignment for conformer C was to a structure that incorporated a γ-turn near its C-terminus but was otherwise held together in which the N- and C-terminal ends are held together largely by a single $NH_3^{+}\cdots O{=}C$ H-bond to the C-terminal COOH group. This conformation is significantly higher in relative energy (9.3 kJ mol^{-1}) and free energy (24.2 kJ mol^{-1}), so much so that its assignment must be considered tentative. Furthermore, there are many structures calculated to have lower free energies at room temperature (where thermal equilibrium would be expected in our room temperature quadrupole linear ion traps), yet we do not see these structures. It is possible that conformer C is a vestige of the

structural preferences present in aqueous solution, particularly in having the NH_3^+ group so asymmetrically bound, with two NH groups available for solvation by H_2O. The *trans*-COOH also may be a unique structural motif facilitated by conformations present in aqueous solution. Despite this intriguing possibility, without further proof, we leave this conformer as a tentative assignment.

V. Conclusions

Cold ion spectroscopy was used to probe the conformational proclivity of ^{L}P and ^{D}P diastereomers with a flexible glycine residue directly C-terminal to the proline. With $[YA^{D}PGA + H]^+$, an unexpected type II β-turn was the single conformer found, and is displaced from the anticipated turn around the ^{D}PG subunit. The type II β-turn is the inverse of the type II′ turn assigned previously to one of the conformations of its close analog, $[YA^{D}PAA + H]^+$. $[YA^{L}PGA + H]^+$ presented with three very different conformers starting with a structure very near to its diastereomer analogue in conformer A, but deformed by the presence of a *cis*-Pro. The two remaining conformers were the globular structure containing a non-proline *cis* amide bond in conformer B, and a tentatively assigned structure unusually high in energy/free energy. The flexibility provided by the G4 residue and the influence of the charge site are principally responsible for formation of these interesting structures. Lastly, we studied in the single-conformation spectroscopy of $[YAA^{D}PGAAA + H]^+$, with its charged N-terminal amine moved further from the site of the anticipated β-turn to see whether by doing so a longer β-hairpin structure might be stabilized in the gas phase. As often happens in these studies, the answer to our initial hypothesis, was 'no', but its alternative was nonetheless interesting in its own right. The single observed conformation incorporated a sequential or concatenated double β-turn involving a type II β-turn about $A^{D}P$ and a type II′ β-turn about GA, leading to a displacement of the peptide backbone laterally without changing the backbone's original direction. This fascinating and potentially useful secondary structural element is an observed but minor contributor to the overlapping β-turns observed in loop regions of X-ray crystal structures in the protein databank.

Conflicts of interest

The authors declare no conflicts.

Acknowledgements

J. T. L., C. H., A. F. B., S. A. M., and T. S. Z. gratefully acknowledge support for this research by the National Science Foundation under grant CHE-1764148. ELS gratefully acknowledges support from NSF *via* Grant No. CHE-1566108. TSZ acknowledges support from the U.S. DOE, Office of Science, Office of Basic Energy Sciences during manuscript preparation at Sandia. Sandia National Laboratories is a multi-mission laboratory managed and operated by National Technology and Engineering Solutions of Sandia, LLC., a wholly owned subsidiary of Honeywell International, Inc., for the U.S. DOE National Nuclear Security Administration under contract DE-NA0003525.

References

1 J. Li, Y. Kuang, Y. Gao, X. Du, J. Shi and B. Xu, D-amino acids boost the selectivity and confer supramolecular hydrogels of a nonsteroidal anti-inflammatory drug (NSAID), *J. Am. Chem. Soc.*, 2013, **135**(2), 542–545.
2 Z. Feng and B. Xu, Inspiration from the mirror: D-amino acid containing peptides in biomedical approaches, *Biomol. Concepts*, 2016, **7**(3), 179–187.
3 D. V. Grishin, D. D. Zhdanov, M. V. Pokrovskaya and N. N. Sokolov, D-amino acids in nature, agriculture and biomedicine, *Front. Life Sci.*, 2019, **13**(1), 11–22.
4 P. A. Novick, D. H. Lopes, K. M. Branson, A. Esteras-Chopo, I. A. Graef, G. Bitan and V. S. Pande, Design of beta-amyloid aggregation inhibitors from a predicted structural motif, *J. Med. Chem.*, 2012, **55**(7), 3002–3010.
5 H. Ohide, Y. Miyoshi, R. Maruyama, K. Hamase and R. Konno, D-Amino acid metabolism in mammals: biosynthesis, degradation and analytical aspects of the metabolic study, *J. Chromatogr. B: Anal. Technol. Biomed. Life Sci.*, 2011, **879**(29), 3162–3168.
6 J. Shi, X. Du, D. Yuan, J. Zhou, N. Zhou, Y. Huang and B. Xu, D-amino acids modulate the cellular response of enzymatic-instructed supramolecular nanofibers of small peptides, *Biomacromolecules*, 2014, **15**(10), 3559–3568.
7 J. Lee and D. G. Lee, Structure-antimicrobial activity relationship between pleurocidin and its enantiomer, *Exp. Mol. Med.*, 2008, **40**(4), 370–376.
8 B. A. Wallace, Common structural features in gramicidin and other ion channels, *BioEssays*, 2000, **22**(3), 227–234.
9 R. Oliva, M. Chino, K. Pane, V. Pistorio, A. De Santis, E. Pizzo, G. D'Errico, V. Pavone, A. Lombardi, P. Del Vecchio, E. Notomista, F. Nastri and L. Petraccone, Exploring the role of unnatural amino acids in antimicrobial peptides, *Sci. Rep.*, 2018, **8**(1), 8888.
10 Z. Luo, X. Zhao and S. Zhang, Structural dynamic of a self-assembling peptide d-EAK16 made of only D-amino acids, *PLoS One*, 2008, **3**(5), e2364.
11 M. Garton, S. Nim, T. A. Stone, K. E. Wang, C. M. Deber and P. M. Kim, Method to generate highly stable D-amino acid analogs of bioactive helical peptides using a mirror image of the entire PDB, *Proc. Natl. Acad. Sci. U. S. A.*, 2018, **115**(7), 1505–1510.
12 E. B. Martin, A. Williams, T. Richey, C. Wooliver, A. Stuckey, J. S. Foster, S. J. Kennel and J. S. Wall, Evaluation of the effect of D-amino acid incorporation into amyloid-reactive peptides, *J. Transl. Med.*, 2017, **15**(1), 247.
13 J. F. Espinosa and S. H. Gellman, A Designedβ-Hairpin Containing a Natural Hydrophobic Cluster, *Angew. Chem., Int. Ed.*, 2000, **39**(13), 2330–2333.

14 J. D. Fisk and S. H. Gellman, A parallel beta-sheet model system that folds in water, *J. Am. Chem. Soc.*, 2001, **123**(2), 343–344.
15 J. D. Fisk, D. R. Powell and S. H. Gellman, Control of Hairpin Formation via Proline Configuration in Parallel β-Sheet Model Systems, *J. Am. Chem. Soc.*, 2000, **122**(23), 5443–5447.
16 H. E. Stanger and S. H. Gellman, Rules for Antiparallel β-Sheet Design: D-Pro-Gly Is Superior tol-Asn-Gly for β-Hairpin Nucleation1, *J. Am. Chem. Soc.*, 1998, **120**(17), 4236–4237.
17 J. D. Fisk, M. A. Schmitt and S. H. Gellman, Thermodynamic analysis of autonomous parallel beta-sheet formation in water, *J. Am. Chem. Soc.*, 2006, **128**(22), 7148–7149.
18 P. S. Walsh, K. N. Blodgett, C. McBurney, S. H. Gellman and T. S. Zwier, Inherent Conformational Preferences of Ac-Gln-Gln-NHBn: Sidechain Hydrogen Bonding Supports a beta-Turn in the Gas Phase, *Angew. Chem., Int. Ed.*, 2016, **55**(47), 14618–14622.
19 H. Fu, G. R. Grimsley, A. Razvi, J. M. Scholtz and C. N. Pace, Increasing protein stability by improving beta-turns, *Proteins*, 2009, **77**(3), 491–498.
20 A. G. de Brevern, Extension of the classical classification of beta-turns, *Sci. Rep.*, 2016, **6**, 33191.
21 W. Kabsch and C. Sander, Dictionary of protein secondary structure: pattern recognition of hydrogen-bonded and geometrical features, *Biopolymers*, 1983, **22**(12), 2577–2637.
22 J. S. Richardson, The anatomy and taxonomy of protein structure, *Adv. Protein Chem.*, 1981, **34**, 167–339.
23 P. K. Baruah, N. K. Sreedevi, R. Gonnade, S. Ravindranathan, K. Damodaran, H. J. Hofmann and G. J. Sanjayan, Enforcing periodic secondary structures in hybrid peptides: a novel hybrid foldamer containing periodic gamma-turn motifs, *J. Org. Chem.*, 2007, **72**(2), 636–639.
24 G. Némethy and M. P. Printz, The γ Turn, a Possible Folded Conformation of the Polypeptide Chain. Comparison with the β Turn, *Macromolecules*, 1972, **5**(6), 755–758.
25 A. C. Gibbs, T. C. Bjorndahl, R. S. Hodges and D. S. Wishart, Probing the structural determinants of type II′ beta-turn formation in peptides and proteins, *J. Am. Chem. Soc.*, 2002, **124**(7), 1203–1213.
26 K. D. Kopple, A. Go and D. R. Pilipauskas, Studies of peptide conformation. Evidence for beta structures in solutions of linear tetrapeptides containing proline, *J. Am. Chem. Soc.*, 1975, **97**(23), 6830–6838.
27 S. R. Trevino, S. Schaefer, J. M. Scholtz and C. N. Pace, Increasing protein conformational stability by optimizing beta-turn sequence, *J. Mol. Biol.*, 2007, **373**(1), 211–218.
28 N. L. Burke, A. F. DeBlase, J. G. Redwine, J. R. Hopkins, S. A. McLuckey and T. S. Zwier, Gas-Phase Folding of a Prototypical Protonated Pentapeptide: Spectroscopic Evidence for Formation of a Charge-Stabilized beta-Hairpin, *J. Am. Chem. Soc.*, 2016, **138**(8), 2849–2857.
29 N. L. Burke, J. G. Redwine, J. C. Dean, S. A. McLuckey and T. S. Zwier, UV and IR spectroscopy of cold protonated leucine enkephalin, *Int. J. Mass Spectrom.*, 2015, **378**, 196–205.
30 O. V. Boyarkin, Cold ion spectroscopy for structural identifications of biomolecules, *Int. Rev. Phys. Chem.*, 2018, **37**(3–4), 559–606.
31 E. Garand, M. Z. Kamrath, P. A. Jordan, A. B. Wolk, C. M. Leavitt, A. B. McCoy, S. J. Miller and M. A. Johnson, Determination of noncovalent docking by infrared spectroscopy of cold gas-phase complexes, *Science*, 2012, **335**(6069), 694–698.
32 A. F. DeBlase, C. P. Harrilal, J. T. Lawler, N. L. Burke, S. A. McLuckey and T. S. Zwier, Conformation-Specific Infrared and Ultraviolet Spectroscopy of Cold [YAPAA + H](+) and [YGPAA + H](+) Ions: A Stereochemical ''Twist'' on the beta-Hairpin Turn, *J. Am. Chem. Soc.*, 2017, **139**(15), 5481–5493.
33 C. P. Harrilal, A. F. DeBlase, J. L. Fischer, J. T. Lawler, S. A. McLuckey and T. S. Zwier, Infrared Population Transfer Spectroscopy of Cryo-Cooled Ions: Quantitative Tests of the Effects of Collisional Cooling on the Room Temperature Conformer Populations, *J. Phys. Chem. A*, 2018, **122**(8), 2096–2107.
34 J. C. Dean, N. L. Burke, J. R. Hopkins, J. G. Redwine, P. V. Ramachandran, S. A. McLuckey and T. S. Zwier, UV photofragmentation and IR spectroscopy of cold, G-type beta-O-4 and beta-beta dilignol-alkali metal complexes: structure and linkage-dependent photofragmentation, *J. Phys. Chem. A*, 2015, **119**(10), 1917–1932.
35 A. Y. Pereverzev and O. V. Boyarkin, Exploring the relevance of gas-phase structures to biology: cold ion spectroscopy of the decapeptide neurokinin A, *Phys. Chem. Chem. Phys.*, 2017, **19**(5), 3468–3472.
36 J. G. Redwine, Z. A. Davis, N. L. Burke, R. A. Oglesbee, S. A. McLuckey and T. S. Zwier, A novel ion trap based tandem mass spectrometer for the spectroscopic study of cold gas phase polyatomic ions, *Int. J. Mass Spectrom.*, 2013, **348**, 9–14.
37 F. A. Londry and J. W. Hager, Mass selective axial ion ejection from a linear quadrupole ion trap, *J. Am. Soc. Mass Spectrom.*, 2003, **14**(10), 1130–1147.
38 F. Mohamadi, N. G. J. Richards, W. C. Guida, R. Liskamp, M. Lipton, C. Caufield, G. Chang, T. Hendrickson and W. C. Still, Macromodel? an integrated software system for modeling organic and bioorganic molecules using molecular mechanics, *J. Comput. Chem.*, 1990, **11**(4), 440–467.
39 A. D. Becke, Density-functional thermochemistry. III. The role of exact exchange, *J. Chem. Phys.*, 1993, **98**(7), 5648–5652.
40 C. Lee, W. Yang and R. G. Parr, Development of the Colle-Salvetti correlation-energy formula into a functional of the electron density, *Phys. Rev. B: Condens. Matter Mater. Phys.*, 1988, **37**(2), 785–789.
41 B. Miehlich, A. Savin, H. Stoll and H. Preuss, Results obtained with the correlation energy density functionals of becke and Lee, Yang and Parr, *Chem. Phys. Lett.*, 1989, **157**(3), 200–206.
42 S. Grimme, S. Ehrlich and L. Goerigk, Effect of the damping function in dispersion corrected density functional theory, *J. Comput. Chem.*, 2011, **32**(7), 1456–1465.

43 M. J. Frisch, G. W. Trucks, H. B. Schlegel, G. E. Scuseria, M. A. Robb, J. R. Cheeseman, G. Scalmani, V. Barone, G. A. Petersson, H. Nakatsuji, X. Li, M. Caricato, A. V. Marenich, J. Bloino, B. G. Janesko, R. Gomperts, B. Mennucci, H. P. Hratchian, J. V. Ortiz, A. F. Izmaylov, J. L. Sonnenberg, D. Williams-Young, F. Ding, F. Lipparini, F. Egidi, J. Goings, B. Peng, A. Petrone, T. Henderson, D. Ranasinghe, V. G. Zakrzewski, J. Gao, N. Rega, G. Zheng, W. Liang, M. Hada, M. Ehara, K. Toyota, R. Fukuda, J. Hasegawa, M. Ishida, T. Nakajima, Y. Honda, O. Kitao, H. Nakai, T. Vreven, K. Throssell, J. A. Montgomery Jr., J. E. Peralta, F. Ogliaro, M. J. Bearpark, J. J. Heyd, E. N. Brothers, K. N. Kudin, V. N. Staroverov, T. A. Keith, R. Kobayashi, J. Normand, K. Raghavachari, A. P. Rendell, J. C. Burant, S. S. Iyengar, J. Tomasi, M. Cossi, J. M. Millam, M. Klene, C. Adamo, R. Cammi, J. W. Ochterski, R. L. Martin, K. Morokuma, O. Farkas, J. B. Foresman and D. J. Fox, *Gaussian 16 Rev. C.01*, Wallingford, CT, 2016.

44 E. L. SibertIII, Modeling vibrational anharmonicity in infrared spectra of high frequency vibrations of polyatomic molecules, *J. Chem. Phys.*, 2019, **150**(9), 090901.

45 J. A. Stearns, S. Mercier, C. Seaiby, M. Guidi, O. V. Boyarkin and T. R. Rizzo, Conformation-Specific Spectroscopy and Photodissociation of Cold, Protonated Tyrosine and Phenylalanine, *J. Am. Chem. Soc.*, 2007, **129**(38), 11814–11820.

46 M. S. Weiss, A. Jabs and R. Hilgenfeld, Peptide bonds revisited, *Nat. Struct. Biol.*, 1998, **5**(8), 676.

47 A. Jabs, M. S. Weiss and R. Hilgenfeld, Non-proline *Cis* peptide bonds in proteins 11, *J. Molecular Biol.*, 1999, **286**(1), 291–304.

48 M. Shapovalov, S. Vucetic and R. L. Dunbrack, Jr., A new clustering and nomenclature for beta turns derived from high-resolution protein structures, *PLoS Comput. Biol.*, 2019, **15**(3), e1006844.

49 W. L. Jorgensen and J. Gao, *Cis-trans* energy difference for the peptide bond in the gas phase and in aqueous solution, *J. Am. Chem. Soc.*, 1988, **110**(13), 4212–4216.